Magnesium Binding to DM-Nitrophen and Its Effect on the Photorelease of Calcium

Richard K. Ayer, Jr. and Robert S. Zucker
Department of Molecular and Cell Biology, University of California, Berkeley, California 94720 USA

ABSTRACT The effect of Mg^{2+} on the process of Ca^{2+} release from the caged Ca^{2+} compound DM-nitrophen (NP) was studied in vitro by steady light UV photolysis of NP in the presence of Ca^{2+} and Mg^{2+}. Ca^{2+} release during photolysis and its relaxation/recovery after photolysis were monitored with the Ca^{2+}-sensitive dye fura-2. Mg^{2+} speeds the photorelease of Ca^{2+} during photolysis and slows the relaxation of Ca^{2+} to new steady-state levels after photolysis. Within the context of a model describing NP photolysis, we determined the on and off rates of Mg^{2+} binding to unphotolyzed NP ($k_{on} = 6.0 \times 10^4$ M^{-1} s^{-1}; $k_{off} = 1.5 \times 10^{-1}$ s^{-1}). Furthermore, to fully account for the slow postphotolysis kinetics of Ca^{2+} in the presence of Mg^{2+} we were forced to add an additional photoproduct to the standard model of NP photolysis. The additional photoproduct is calculated to have a Ca^{2+} affinity of 13.3 μM and is hypothesized to be produced by the photolysis of free or Mg^{2+}-bound NP; photolysis of Ca^{2+}-bound NP produces the previously documented 3 mM Ca^{2+} affinity photoproduct.

INTRODUCTION

Caged Ca^{2+} compounds, molecules that can rapidly flood a cell with Ca^{2+} after exposure to ultraviolet light (Tsien and Zucker, 1986; Kaplan and Ellis-Davies, 1988), have enjoyed extensive and increasing use since their development in the late 1980s (Zucker, 1994). Recently, several papers studying the properties of Ca^{2+} release from various caged compounds have appeared (Landò and Zucker, 1989; Zucker, 1993; Escobar et al., 1995, 1997; Ellis-Davies et al., 1996; Parsons et al., 1996; Xu et al., 1997). DM-nitrophen (NP) and nitrophenyl-EGTA (NP-EGTA), two caged Ca^{2+} compounds regularly used for systematic manipulation of Ca^{2+}, are capable of raising Ca^{2+} from rest (100 nM) to levels in the range of 50–100 μM (Kaplan and Ellis-Davies, 1988; Ellis-Davies and Kaplan, 1994). By contrast, the third regularly used cage, nitr-5 (Adams et al., 1988) raises Ca^{2+} into the range of 1–5 μM. Although there are many experiments where nitr-5 is useful (e.g., Cash et al., 1996; Neveu and Zucker, 1996), NP and NP-EGTA remain the cages of choice when large elevations in Ca^{2+} are necessary (Ellis-Davies and Kaplan, 1994; see Zucker, 1994 for review).

Because of its roughly fivefold higher absorbance when compared to NP-EGTA, NP allows for more efficient and faster photolysis and thus higher Ca^{2+} levels at a given UV light level (Parsons et al., 1996). This benefit is, however, somewhat counterbalanced by the relative lack of specificity of Ca^{2+} binding for NP (Kaplan and Ellis-Davies, 1988; Ellis-Davies and Kaplan, 1994; Parsons et al., 1996). While NP binds Ca^{2+} in the nanomolar range and NP-EGTA in the 100-nanomolar range, NP has a micromolar affinity for Mg^{2+} while the affinity of NP-EGTA for the alternative ligand is in the millimolar range. NP-EGTA effectively does not bind Mg^{2+}. The high affinity of NP for Mg^{2+} has plagued the field and was the major force behind the development of the newer NP-EGTA (Ellis-Davies and Kaplan, 1994). However, because of its higher absorbance, NP has remained popular (Kamiya and Zucker, 1994; Parsons et al., 1995; Xu et al., 1997). Often, experiments can be accomplished in semi-intact preparations where Mg^{2+} can be omitted and the NP chemistry thus simplified (see, for example, Neher and Zucker, 1993; Thomas et al., 1993; Heidelberger et al., 1994). However, in a number of cases, Mg^{2+} is either critical for the process under examination or its levels cannot be controlled by the experimenter (Delaney and Zucker, 1990; Mulkey and Zucker, 1993; Kamiya and Zucker, 1994; Landò and Zucker, 1994; Gillis et al., 1996; Patel et al., 1996). Thus, there is clearly a need to understand the Ca^{2+} release process in the presence of physiological levels of Mg^{2+}.

To date, the literature examining the photochemistry and kinetics of NP has not looked at the properties of the chelator in the presence of Mg^{2+}. In fact, it has never been demonstrated that Mg^{2+} has any effect on release kinetics or on Ca^{2+} levels reached during photolysis. As the proper use of NP in many experiments requires an understanding of Mg^{2+}-NP interactions, we have pursued a series of experiments designed to monitor the effects of Mg^{2+} and to characterize the kinetics of Mg^{2+} binding. This will be done in the context of a model that takes into account Mg-NP interactions in addition to the better-studied Ca-NP interactions.

Mg-NP interactions are slow, their on-rates limited by the slow removal of H_2O from hydrated Mg^{2+} (Hague, 1977). We are thus able to study Mg-NP binding during photolysis produced by relatively long-lasting (~1 s) steady light pulses. This has two very distinct advantages. The first is

Received for publication 2 February 1999 and in final form 1 September 1999.

Address reprint requests to Dr. Robert Zucker, University of California, Molecular and Cell Biology Department, 111 Life Sciences Addition, Berkeley, CA 94720-3200. Tel.: 510-642-3407; Fax: 510-643-6791; E-mail: zucker@socrates.berkeley.edu.

R. K. Ayer, Jr.'s present address is Sutter Instrument Company, Novato, CA 94949.

0006-3495/99/12/3384/10 $2.00

practical. Past work from this laboratory (Kamiya and Zucker, 1994; Landò and Zucker, 1994; Mulkey and Zucker, 1993) used similar NP photolysis paradigms to study transmission at the crayfish neuromuscular junction. We hope to more completely characterize the Ca^{2+} levels produced by NP photolysis in these experiments. The second advantage is procedural. As photolysis is slow, we can monitor its progress quantitatively during photolysis (Xu et al., 1997). The nature of presently available dyes is such that they are still not fast enough to monitor the large, fast Ca^{2+} transients that are produced by laser or flash photolysis (Ellis-Davies et al., 1996; Escobar et al., 1997). By keeping concentrations of the Ca^{2+} indicator low—in our case 1% of cage concentration—we can assure a fluorescent dye response that accurately tracks changes in Ca^{2+} levels induced by slow photolysis.

The results presented in this paper suggest that the models currently used to describe the release of calcium from NP (Zucker, 1993; Ellis-Davies et al., 1996; Escobar et al., 1997) must be revised to describe the kinetics of Mg^{2+} binding to the cage. The revision requires the addition of a secondary photoproduct that is produced when NP is either free or bound to Mg^{2+}. In addition to the fact that this model more completely describes NP photolysis in the presence of Mg^{2+}, it is also attractive in that it explains the existence of differentially absorbing photoproducts that were seen when NP was photolyzed in either the presence or absence of Ca^{2+} (Kaplan and Ellis-Davies, 1988).

MATERIALS AND METHODS

Solutions

All experiments were conducted using a solution containing a mixture (concentrations in mM) of K_4NP, 5.0; $CaCl_2$, 2.0; KCl, 79; KHepes, 50; ionic strength 135 mM, pH 7.3. When Mg^{2+} was present it was added at 2.0 mM as $MgCl_2$, and KCl was adjusted to keep ionic strength constant. Fura-2 was used at a concentration of 0.05 mM.

To estimate the concentration of the NP used in this study, we performed a Ca^{2+} titration (Bers, 1982) of the unphotolyzed stock (nominally 75 mM) using a Ca^{2+} electrode calibrated using solutions of known Ca^{2+}. This analysis showed that the stock was actually 60 mM. All solutions were corrected to reflect this concentration. NP was a generous gift of Graham Ellis-Davies. Fura-2 was from Molecular Probes (Eugene, OR). Ca^{2+} was added to all solutions using a 100 mM standard $CaCl_2$ solution (Orion, Boston, MA). $MgCl_2$ was added using a 4.9 M stock solution (Sigma, St. Louis, MO) to minimize $MgCl_2$ hydration errors. All other reagents were obtained from Sigma.

Cuvettes

All experiments were done in glass microcuvettes, 20 μm pathlength, 200 μm wide (VitroCom, Mountain Lakes, NJ). They were broken into lengths of 5–10 mm, filled by capillary action, and placed on a glass-bottom petri dish under a layer of nonfluorescent light mineral oil and then moved to the fluorescence microscope.

Photolysis and fura-2 measurement

A single light source was used for both photolysis of NP and excitation of fura-2. The lamp was an ILC Cermax 150 W xenon arc bulb (Model LX150UV; ILC Technologies, Sunnyvale, CA), driven by an ILC power supply (Model PS 150-9). The light was focused into the epifluorescence port of a Nikon Optiphot compound microscope. The epifluorescence light attachment carried standard Nikon neutral density filters (Nikon ND2 and ND4) and also contained an iris diaphragm to delimit the field illuminated by the ILC light.

Two additional items were interposed in the light path between the lamp and the entrance to the epifluorescence attachment. The first was an electronically controlled shutter (Model VS25S1ZMOL, Uniblitz, Rochester, NY). The second was a sliding filter holder that carried the two fura-2 excitation filters: 1) a custom-made 382-nm center wavelength, 15-nm bandwidth filter (Chroma Technology, Brattleboro, VT) and 2) a standard 360-nm center wavelength, 10-nm bandwidth filter (Omega Optical, Brattleboro, VT). The 382-nm filter was used for simultaneous fura-2 excitation and photolysis, while the 360-nm filter was used for a Ca^{2+}-independent ratio measurement when required. After passing through the excitation filters, UV light was reflected by a Nikon dichroic mirror (DM455); light below its 455 nm cutoff was directed through the microscope objective to the cuvette. Fluorescence excited by UV wavelengths and emitted by the fura-2 passed through the dichroic and a 530-nm center wavelength, 20-nm bandpass emitter filter before continuing to either the microscope eyepieces or the photomultiplier detector.

The light source, when used in combination with the 382-nm filter and with a 40X-UV Olympus long working distance water immersion lens (WPlan FL40X UV, NA 0.7) was capable of photolyzing 50% of NP in 320 ms, corresponding to a photolysis rate of 2.39 s^{-1}. For most of the experiments described here, the light was decreased by closing the iris diaphragm and defocusing the microscope stage (see below). In Fig. 1, the light was additionally decreased by a 50% transmission neutral density filter.

Photomultiplier detection of fluorescence

All experiments detailed in this study used a Hamamatsu photomultiplier tube (R928HA) to detect the light emitted by fura-2. The photomultiplier tube (PMT) was mounted on the camera port of the Nikon microscope. A Nikon diaphragm cassette holder with rectangular diaphragm was interposed in the light path before the PMT to restrict the field of the objective to be detected before the light was measured by the PMT. A second Uniblitz shutter was interposed in the PMT light path to allow light to reach the PMT only during the time that the fura-2 was emitting light. The output of the PMT was connected to a current-to-voltage converter and fed into a data acquisition system (Digidata 1200 AD/DA interface controlled by pClamp6, Axon Instruments, Foster City, CA). pClamp6 was used to control opening of both shutters in conjunction with digital pulse generator (Master 8, A.M.P.I., Jerusalem, Israel). Records were corrected for background fluorescence.

Elimination of diffusion artifacts

The limitation of photolysis to the area circumscribed by a 40× microscope objective, roughly a 400-μm-diameter circle, introduces potential difficulties for photolysis experiments. First, it is difficult to produce a short cuvette that fits entirely within the 400-μm circle encompassed by the objective field of view. Furthermore, nonuniformities in illumination forced us to use an even more restricted photolysis field of a 250-μm-diameter circle (delimited by the iris in the epifluorescence light path). Thus we measured fluorescence from a small portion of the larger photolyzed region in a way that minimizes changes that can occur as the result of unphotolyzed NP diffusing into the measurement area. The cuvette thickness is 20 μm while its width is 200 μm; both of these dimensions fall within the photolysis field. The length of the cuvette, however, cannot be easily limited to under 1 mm. Instead, we maximized the photolyzed area while minimizing the measurement area to a small 730 μm^2 square in the center of the fluorescence field (delimited by the rectangular diaphragm in the photomultiplier light path). Irregularities in illumination were mini-

mized by defocusing the microscope stage (roughly one turn of the fine focus, 100 μm), and by not using the smallest possible measurement region.

Steady, high Ca^{2+} levels were seen for at least 10 s after complete photolysis. Under these conditions, any variation in Ca^{2+} levels after photolysis would have to be due to diffusion from outside the photolyzed area, or from an area of the photolyzed field with a different amount of photolysis due to intensity differences. Using the equation $r^2 = 2Dt$ for one-dimensional diffusion, we can calculate an average diffusion time (t) for a radius (r) of 125 μm and a diffusion constant ($D = 6 \times 10^{-6}$ cm^2/s) for a small molecule like Ca^{2+}. Using these values gives $t = 13$ s, in good agreement with the empirically determined value.

The use of long cuvette pieces allowed us to collect several photolysis-recovery records per cuvette (see Fig. 3), as long as the amount of NP photolyzed in a single episode was small. The records in Fig. 3 photolyze 23% of the NP in a single run. Under these conditions, using a cuvette that was 20–40 times as long as the 250-μm photolysis spot, up to 10 photolysis events could be collected per cuvette. A ratiometric determination of Ca^{2+} level was made just before each photolysis episode. Even a slight increase in pre-photolysis fura-2 ratio predicted that the Ca^{2+} during the episode would rise more quickly than normal, due to the presence of prephotolyzed NP. Records showing such behavior were not used in this analysis.

Ratiometric Ca^{2+} measurements followed the well-established methods of Grynkiewicz et al. (1985). In addition, we followed the work of Henke et al. (1996) who demonstrated that fura-2 exhibits two Ca^{2+} binding sites. These authors found that a free calcium concentration of ~10 μM saturated the higher affinity site while remaining below the K_d of the lower affinity site. The free calcium level at the end of "complete" photolysis of the experimental solution outlined above is predicted to be in this range. Using 10 μM as the saturating calcium concentration, a five-point calibration of fura-2 in the presence of NP (Zucker, 1992; Neher and Zucker, 1993) was performed to determine R_{min}, R_{max}, and K_d for fura-2. R_{min} and R_{max} values of 0.275 and 0.916 were obtained. The K_d, derived using Eq. 5 of Grynkiewicz et al. (1985), was 0.73 μM. The high value of K_d obtained is expected from the known interactions between NP and fura-2 (Zucker, 1992).

For the experimental solution detailed above, the calcium level expected before photolysis, or at the onset of photolysis before significant calcium is released, is predicted to be near 10 nM. The above calibration gives initial calcium levels for the data of Fig. 3 on the order of 100–200 nM. To match the measured initial calcium levels for each exposure to the predicted value of 10 nM, R_{min} was varied by a small amount, always $<5\%$. The exact values of R_{min} used are given in the figure legends.

At the end of the 10 s photolysis shown in Fig. 4, values of R approached or exceeded R_{max}. As this produces meaningless calculated values of calcium, the value of R_{max} was increased an arbitrary amount (to a value of 1.00) for the data in this figure only. As will be discussed below, adjustments to R_{min} and R_{max} do not affect the Mg^{2+}/NP binding constants obtained through modeling.

To demonstrate raw data and allow understanding of how the data set was constructed, records in this paper express Ca^{2+} levels in two ways. Changes in fura-2 fluorescence intensity at 382 nm (raw data) are shown in Figs. 1 and 2 *A*. In the remaining figures (2 *B*, 3, and 4), we show changes in $[Ca^{2+}]$ as predicted using the above calibration.

As the fura-2 signal at 360 nm is independent of $[Ca^{2+}]$ (Grynkiewicz et al., 1985), we measured the 360-nm signal just before photolysis. In some experiments, it was confirmed that the 360-nm fluorescence remained unchanged after photolysis of NP. Subsequent records of fura-2 fluorescence at 382 nm obtained during photolysis—and during the post-photolysis recovery—can thus be converted to a time-varying ratio and then a $[Ca^{2+}]$ time course can be calculated.

Modeling

All computer modeling was programmed in MicroSoft Professional Basic 7.0 running in a DOS window under Windows95 on a Pentium II processor. Variable parameters were optimized by trial and error.

RESULTS

Fig. 1 compares the photolysis records from cuvettes in the presence and absence of Mg^{2+}. In this figure the data presented are the fura-2 fluorescence intensity excited by UV light centered at 382 nm with a bandwidth of 15 nm. As the fura-2 signal intensity at wavelengths longer than 360 nm is inversely proportional to $[Ca^{2+}]$ (Grynkiewicz et al., 1985), increases in $[Ca^{2+}]$ are seen as decreases in fluorescence intensity.

Mg^{2+} has a powerful effect on the $[Ca^{2+}]$ rise produced by photolysis. The Mg^{2+}-free record (upper trace, Fig. 1) drops to half its initial value at ~4.5 s, or after ~4 s of photolysis. The fast increase in Ca^{2+} occurs at the point where remaining unphotolyzed NP drops below the total Ca^{2+} concentration (i.e., after 3 mM NP has been photolyzed). Assuming that Ca^{2+}-free and Ca^{2+}-bound NP are photolyzed at similar rates, we can determine a photolysis rate of 0.23 s^{-1} (Zucker, 1993). Here photolysis rate is limited by the intensity of the light, and is not a measure of the intrinsic photolysis rate occurring after absorption of a photon (Ellis-Davies et al., 1996).

By contrast, the cuvette containing Mg^{2+}, in this case 2 mM (lower trace, Fig. 1), shows a faster increase in $[Ca^{2+}]$. Although this behavior has long been predicted from the competition of Mg^{2+} and Ca^{2+} for the cationic binding site of NP, this is the first demonstration that Mg^{2+} changes the kinetics of $[Ca^{2+}]$ elevation by NP photolysis. In this case, fluorescence intensity drops to the same midpoint after only 2.5 s of photolysis. The concentration of Mg^{2+} used in this experiment (2 mM) is similar to intracellular levels, while the NP and Ca^{2+} concentrations are near values typically reached in cells we inject. The pronounced difference of the records in the absence and presence of Mg^{2+} emphasizes the need for taking Mg^{2+} binding into account when trying

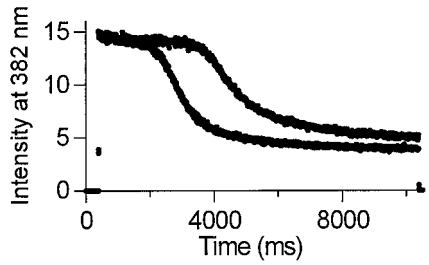

FIGURE 1 Steady light photolysis of Ca-NP in the absence or presence of Mg^{2+}. Records show the fura-2 fluorescence and simultaneous photolysis of cuvettes excited at 382 nm and monitored using a photomultiplier tube. In both traces, cuvettes contained an identical mixture of (in mM) NP, 5.0; Ca^{2+}, 2.0; and fura-2, 0.05. The lower trace shows the faster increase in $[Ca^{2+}]$ (decrease in fluorescence) because the cuvette it was recorded from contained 2.0 mM Mg^{2+} in addition to the other contents. Light levels are initially at zero intensity, then jump to a large value as the shutter in the excitation/photolysis light path opens at 400 ms. Fura-2 intensity at 382 nm then decreases with the Ca^{2+} increase caused by photolysis. Finally, records drop back to zero intensity after 10 s when the shutter closes. Light levels for this figure were limited by 50% using a neutral density filter; each trace is the average of 10 similar exposures.

to estimate the behavior of Ca^{2+} release from photolyzed NP in the presence of physiological concentrations of Mg^{2+}.

During photolysis, changes in [Ca^{2+}] are determined by the simultaneous interactions of multiple buffer systems. These interactions are further complicated by the fact that the concentrations of two of the buffers, NP and its photoproduct(s), are changing. At the end of partial photolysis, [Ca^{2+}] relaxes to a lower level as recently released Ca^{2+} displaces Mg^{2+} bound to unphotolyzed NP. The relaxation kinetics are determined by the same buffers as during photolysis, but the buffer concentrations remain fixed for the remainder of the record. Therefore, for simplicity we chose to characterize Mg^{2+} effects during the recovery phase. This was done by using fixed-length (1–1.5- s) steady light pulses to photolyze, followed by 10-ms light pulses at various time points to monitor the fura-2 signal ([Ca^{2+}] level) during recovery or relaxation (see Fig. 2 *A, inset*). The monitoring pulses were kept short to minimize additional photolysis.

Initially, we compared recovery in the absence and presence of Mg^{2+} to confirm the expectation that recovery would be slower in the presence of Mg^{2+} (Zucker, 1993). This can be seen clearly in Fig. 2 *B*, which shows the relaxation of the monitored fura-2 signal as a function of time after the end of photolysis in the presence or absence of Mg^{2+}. In this figure we have converted fluorescence intensity to [Ca^{2+}] levels so that the several different records can be more easily compared. An equal length photolysis pulse (1.2 s) is given to both samples and the recovery is compared. As can be seen, the recovery in the presence of Mg^{2+} is clearly slower. A single exponential fit to the data gives recovery time constants of 391 ms in the presence of Mg^{2+} and 17 ms in the absence Mg^{2+}. Note that the 17-ms time constant is of limited value due to the 10-ms shutter open time used to generate time points during recovery. At this level of resolution, the recovery in the absence of Mg^{2+} is instantaneous.

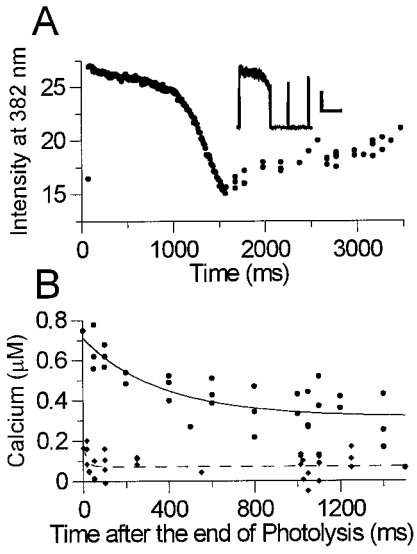

FIGURE 2 The addition of Mg^{2+} slows recovery of Ca^{2+} levels after photolysis of NP-Ca^{2+}. Raw data records were collected as indicated in the inset to (*A*) (scale bars: 1 s; 10 intensity units). The shutters in front of the UV lamp and the photomultiplier tube were opened for a specified time (here 1.5 s) to allow a fixed amount of photolysis to occur. Both shutters were closed and then reopened for two brief periods (10 ms each) to monitor the recovery of Ca^{2+} after the photolysis event. (*A*) Composite record generated by averaging 18 records similar to the inset. By varying the length of time from the end of the photolysis episode to the monitoring pulse(s), the time course of the recovery or relaxation can be traced out. (*B*) Ca^{2+} recovery in the presence (*filled circles*) or absence (*filled diamonds*) of Mg^{2+} are compared after a 1.2-s photolysis event. Ca^{2+} levels are calculated using the ratio of the intensity at 360 nm just before the exposure to the intensity at 382 nm during the exposure. The solid curves are single exponential fits to the data; recovery time constants: 391 ms in the presence of Mg^{2+} (*solid curve*), 17 ms in the absence of Mg^{2+} (*dashed curve*, 17 ms time constant at or near minimum value resolvable with a 10-ms shutter open time). Cuvettes contained an identical mixture of (in mM) NP, 5.0; Ca^{2+}, 2.0; and fura-2, 0.05; with or without 2.0 mM Mg^{2+}.

The time course of the recovery process is expected to be a function of the rates of binding and unbinding of Ca^{2+} and Mg^{2+} from NP. Because the binding rates are second-order, they are also dependent on the postphotolysis levels of Ca^{2+} and Mg^{2+}. The recovery will also be dependent on indicator binding. However, inasmuch as the relaxation time courses are slow when compared to Ca^{2+} fura-2 binding (Jackson et al., 1987; Kao and Tsien, 1988), indicator binding will have little effect on the time course of recovery as long as indicator concentration is kept low with respect to cage concentration. Although it might be expected from casual analysis, it is not true that the slow recovery in the presence of Mg^{2+} is directly related to the slow off rate for Mg^{2+} from Mg-NP. In fact, due to their high concentrations at the end of photolysis, both Ca^{2+} and Mg^{2+} unbind and rebind at similar rates (1–10 s^{-1}), and thus no single rate dominates the recovery time constant of the process. For this reason we cannot determine Mg-NP binding rates in a model-independent fashion. We first present the data detailing the recovery of Ca^{2+} after photolysis and then describe the model required to fit the data.

Fig. 3 shows the recovery of Ca^{2+} levels, in the presence of Mg^{2+}, after photolysis pulses of three durations: 1.0, 1.2, and 1.5 s (*filled circles*, panels *A–C*, respectively). As can be seen, increasing the amount of NP photolyzed slows recovery time after photolysis. Each panel is a composite of a number of experiments; the dense, ascending portion at the onset shows averaged increase in Ca^{2+} during photolysis. This is followed by single, or in some cases averaged, time points that track the time course of recovery after photolysis.

To test our model further, we produced an additional type of data. Fig. 4 shows the average response to a longer photolysis episode (10 s) in the presence of Mg^{2+} (*filled circles*). These data allow us to test the model under cases of more complete NP photolysis.

Modeling

Recovery of Ca^{2+} to low levels after photolysis, as well as increase of Ca^{2+} during photolysis, was initially modeled

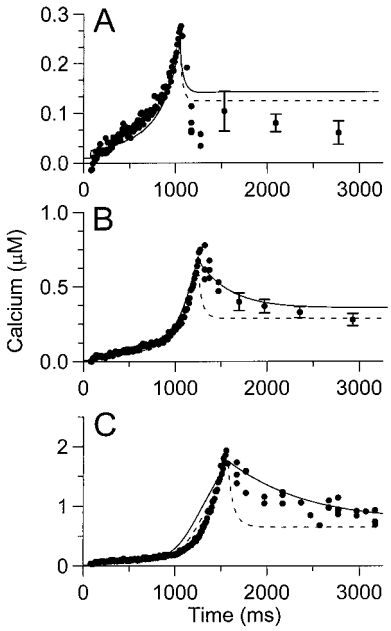

FIGURE 3 Recovery becomes slower and less complete with increasing photolysis. The three panels show [Ca^{2+}] levels both during and after photolysis exposures of three durations: (*A*) 1.0 s; (*B*) 1.2 s; and (*C*) 1.5 s. In all records, cuvettes contained an identical mixture of (in mM) NP, 5.0; Ca^{2+}, 2.0; Mg^{2+}, 2.0; and fura-2, 0.05. The filled circles are the data and the dashed and solid curves are the fits of Schemes 1 and 2, respectively (see Modeling). Raw data records were collected as indicated in Fig. 2 *A*. The recovery is very fast after 1.0 s (*A*), becomes much slower after 1.2 s (*B*), and shows a very slow recovery after 1.5 s of photolysis (*C*). Records are the composite of 18 trials in (*A*) and (*C*), and 20 trials for (*B*). During photolysis (the ascending part of the curve) we show the average of all data trials. During recovery we show single recovery data points and/or binned and averaged data. To remove some of variation of individual trials during recovery, the intensity level at the end of photolysis was measured and used to normalize the intensity of recovery data points for each individual record. When averaged, recovery points are shown as mean ± SE; n = 4–13 points per bin. R_{min} for the fura-2 calibration was altered a small amount to make initial Ca^{2+} levels of the data match those predicted by the model: values used for R_{min} are 0.286, 0.288, and 0.277 for panels *A–C*, respectively.

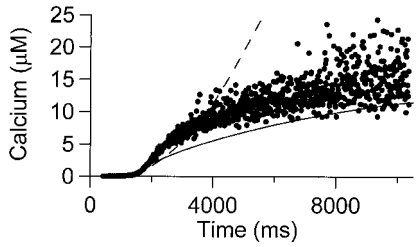

FIGURE 4 Photolysis for a longer period raises Ca^{2+} levels to nearly saturate fura-2 and produces data that further constrain photolysis models. The data set, shown here in the filled circles, is the average increase in [Ca^{2+}] of four similar photolysis episodes, each lasting 10 s. Recovery, not shown, is so slow after this length of photolysis that it would be severely contaminated with diffusional processes that also occur in the cuvette. Dashed and solid lines are fits to the data using Schemes 1 and 2, respectively. These data approach the fura-2 R_{max} at the end of the exposure. To estimate Ca^{2+} levels for these data, R_{max} was increased to 1.00.

using a scheme previously developed in this lab (Delaney and Zucker, 1990; Zucker, 1993) and generally similar to that used by others (Ellis-Davies et al., 1996: Escobar et al., 1997). The scheme is diagrammed as Scheme 1 on the following page.

Briefly, the model allows for photocleavage of individual molecules of NP (NP) into two identical molecules of low-affinity photoproduct (2 PP). NP can be photolyzed in its free, Ca^{2+}-bound (CaNP), or Mg^{2+}-bound forms (MgNP). If either Ca^{2+} or Mg^{2+} is bound to NP, the ion is released to free solution after photolysis. Forward (α) and backward (β) rates for the binding of Ca^{2+} and Mg^{2+} to NP and PP, and for binding to the fluorescent indicator fura-2 (F) are given in Table 1. We used the fura-2 dissociation rate from Jackson et al. (1987) and Kao and Tsien (1988), and calculated the binding rate from this and our estimate of K_d in the presence of NP (see Methods).

Before we detail the Mg^{2+} binding rates we have determined by fitting Scheme 1 to our data, it is useful to describe several changes in the Ca^{2+} binding and photolysis rates that we have altered from previous models. First, we take into account the new CaNP binding rates as determined by Escobar et al. (1997) and Xu et al. (1997), which are ~⅓ those estimated by Ellis-Davies et al. (1996) and substantially faster than those estimated by Zucker (1993); threefold changes in these kinetics have little effect on our derived estimates of Mg-NP binding kinetics. Second, we have simplified the mechanism of photolysis in our original model. Based on measurements of the absorbance changes of NP or Ca-NP and its photoproducts, Zucker (1993) proposed a 2.5-fold faster rate of photolysis for NP when bound to Ca^{2+} as compared to free NP. However, others have used identical rates of photolysis for both bound and free NP (Ellis-Davies et al., 1996; Escobar et al., 1997, but see Xu et al., 1997), and we have made this assumption in analyzing the present data. Finally, we chose to use Neher and Zucker's (1993) value (250 μM) for the Ca^{2+} dissociation constant of photolyzed NP. This is a 12-fold higher affinity than the value, 3 mM, published initially by Kaplan and Ellis-Davies (1988). A 3 mM affinity for Ca^{2+} binding to PP was also used by Ellis-Davies et al. (1996) while a 2.5 mM affinity was used by Escobar et al. (1997). However, in our hands, [Ca^{2+}] levels never reached those predicted by an NP photoproduct with a K_d in the range of 2.5–3 mM (see Discussion for additional detail).

Using Scheme 1, we fit our experimental results to produce a model of NP photolysis that describes Ca^{2+} release in the presence of Mg^{2+}. The only free parameter was the rate of Mg^{2+} binding to NP (α_2) and its photoproduct (α_4). The photolysis rate, R, was allowed to vary (in practice $<\pm 2\%$ was required) to account for sample-to-sample variability in the magnitude of the light seen by the cuvette due to somewhat variable defocusing (see Methods). Also, as detailed in the Methods section, the calcium level calculated for the data at the onset of photolysis was set to the value predicted by the model by varying the value of R_{min}.

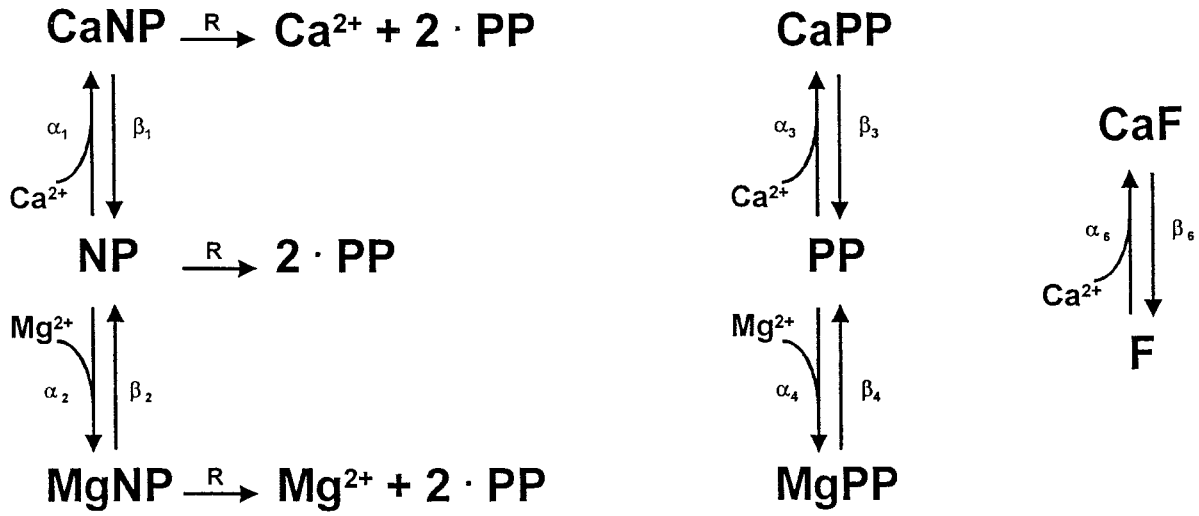

Scheme 1 The rates given with this scheme are given in Table 1.

We chose as a first approximation to set Mg-NP binding rates to reflect the slow dehydration of Mg^{2+}. In many systems (Hague, 1977) it has been shown that Mg^{2+} binding is largely limited by the rate of dehydration of Mg^{2+} before binding to a specific site. Thus, maximal Mg^{2+} binding rates set by water displacement are on the order of 5×10^5 M^{-1} s^{-1}. Using this on-rate, the corresponding off-rate can be determined as off-rate = $K_d \cdot$ on-rate. For $K_d = 2.5$ μM (Kaplan and Ellis-Davies, 1988), the off-rate is equal to 1.25 s^{-1}. Using these rates as a guide, we set out to determine the MgNP binding rates that best fit the data.

The model, using the MgNP binding rates given in Table 1, produces satisfactory fits to fluorescence measurements during photolysis events lasting up to 3 s (Figs. 3 and 4). However, the model describes postphotolysis recovery only after short photolysis episodes (1.0 s; Fig. 3 *A*). The fits using this scheme are shown in Fig. 3 as dashed lines. As photolysis times increased to longer pulses (1.2–1.5 ms; Fig. 3, *B* and *C*), the fit to the recovery period became increasingly poor and much faster than the data. The rates used in Scheme 1 were varied extensively, and variations were tried in which the photolysis rate *R* was different for the different species produced (NP, CaNP, and MgNP). However, none of these manipulations produced predictions that properly fit the slow recovery after longer photolysis episodes.

One way in which we can slow down Ca^{2+} relaxations after more substantial photolysis is to posit the presence of an additional medium-affinity Ca^{2+} buffer with slower kinetics (in particular, slower off-rate) formed as a photoproduct. This photoproduct would slow down Ca^{2+} relaxations in the same way that too much high affinity Ca^{2+} indicator inhibits the ability to measure fast Ca^{2+} transients. There are at least two ways such a buffer might be created during NP photolysis. First, we might imagine that the photolysis reaction occurs in steps: after an initial photolysis event occurs, a medium-affinity buffer species is created which then spontaneously decays to the final low-affinity photoproduct. At least one major problem exists with such a mechanism: the rate of spontaneous decay would have to be very slow to produce the relaxations and the apparent steady-state elevated Ca^{2+} we see in our data (Fig. 3 *C*). Initial attempts to use such a model did show improved fitting, however; they required spontaneous breakdown rates as slow as 15 s^{-1} to fit the data. Such a slow production of photoproduct is not consistent with measurements of rate of [Ca^{2+}] change in response to flash photolysis (Ellis-Davies et al., 1996).

An alternative mechanism to create an additional Ca^{2+} buffer during photolysis assumes that photolysis occurs along two different pathways, each of which produces a different, stable photoproduct. Such a scheme is represented as Scheme 2 on the following page.

Scheme 2 is similar to the conventional Scheme 1 shown above. The major difference is that NP can be photolyzed to two different stable photoproducts, PP1 and PP2. PP1 is

TABLE 1 Rates for scheme 1

Ca-NP		Mg-NP		Ca-PP		Mg-PP		Ca-F	
α^1	3.00×10^7	α_2	5.00×10^5	α_3	3.00×10^7	α_4	5.00×10^5	α_6	1.22×10^8
β_1	1.50×10^{-1}	β_2	1.25×10^0	β_3	7.50×10^3	β_4	1.50×10^3	β_6	9.00×10^1
K_{d1}	5.00×10^{-9}	K_{d2}	2.50×10^{-6}	K_{d3}	2.50×10^{-4}	K_{d4}	3.00×10^{-3}	K_{d6}	7.3×10^{-7}

Values are given in the following units: α (M^{-1} s^{-1}); β (s^{-1}); K_d (M). The total concentrations used in the model were as follows (in mM): NP, 5.0; Ca^{2+}, 2.0; Mg^{2+}, 2.0; fura-2, 0.05. The photolysis rate, *R*, used to fit the data in the presence of Mg^{2+} was allowed to vary a small amount (0.22–0.24) to account for exposure to exposure variability due to differences in defocusing.

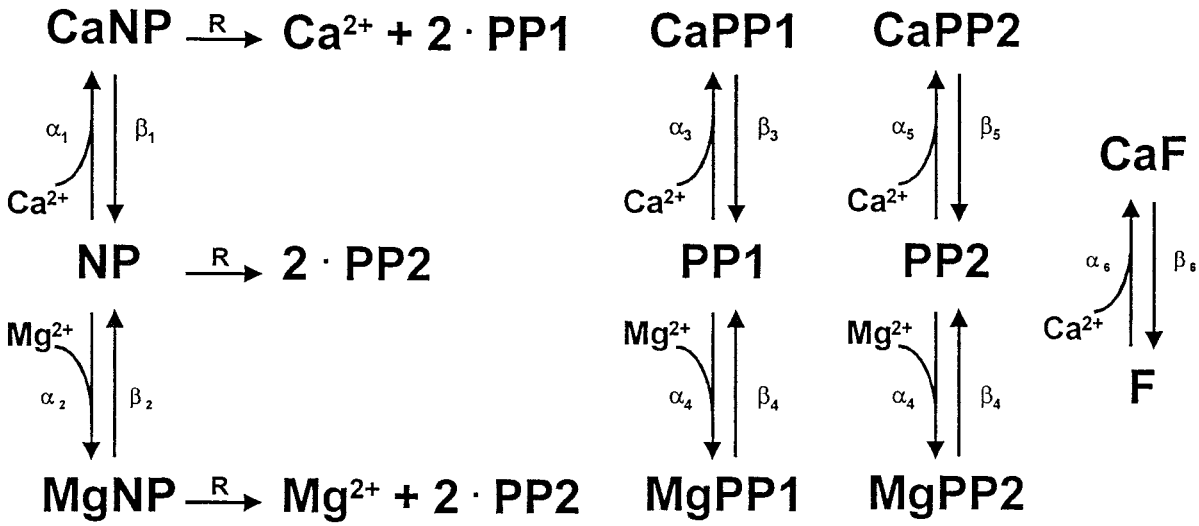

Scheme 2 The rates given with this scheme are given in Table 2.

produced by the photolysis of CaNP, or Ca^{2+}-bound NP, and PP2 is produced by the photolysis of either free NP or MgNP. The only difference between PP1 and PP2 is their Ca^{2+} affinity. PP1 is given the 3 mM Ca^{2+} affinity measured by Kaplan and Ellis-Davies (1988); they photolyzed NP in the presence of saturating concentrations of Ca^{2+} and then determined the affinity of the resulting photoproduct. In this case Scheme 2 would predict that the total photolysis product was in the form PP1.

We have used our data, specifically the steady-state Ca^{2+} level at the end of the postphotolysis relaxations in Fig. 3, *A–C* to effectively titrate the buffer PP2 in the presence of the other buffer species, all of known affinity. This is similar in principle to the approach used by Xu et al. (1997) to determine the affinity of the intracellular buffer in chromaffin cells. As indicated in Table 2, we obtain a Ca^{2+} K_d for PP2 of 13.3 μM. The K_d for Mg^{2+} binding to both PP1 and PP2 was assumed to be equivalent to the value used for PP in Scheme 1.

This leaves us with a model with all rates determined except for the on- and off-rates of Mg^{2+} binding to NP. In Scheme 2, altering these rates (α_2 and β_2) has a strong effect on predicted [Ca^{2+}] recovery after 1.2–1.5-s photolysis events. The best-fitting values associated with Mg^{2+} binding to NP were $\alpha_2 = 6 \times 10^4\ M^{-1}\ s^{-1}$; $\beta_2 = 1.5 \times 10^{-1}\ s^{-1}$.

As indicated by the solid curves in Fig. 3, Scheme 2 fits the slow recovery of Ca^{2+} levels after photolysis. We believe this justifies the use of a photolysis scheme where NP photolyzes into two different photoproducts.

Scheme 2 also does a better job than Scheme 1 in predicting Ca^{2+} levels and kinetics during the more complete continuous photolysis shown in Fig. 4. The calcium levels predicted for the Scheme 1 fit exceed 25 μM after ~5 s and reach over 50 μM at by the end of the exposure. Calcium levels are not well-defined for this data set because fluorescence ratios approach R_{max} toward the end of the exposure. Thus, the fact that Scheme 2 approximates the data is not strong conformation of the model: if one chooses a larger value of R_{max}, the data can be made to match the Scheme 2 fit even more closely. However, there is no value of R_{max} that can be chosen such that the data reach the calcium levels predicted by Scheme 1.

DISCUSSION

We have measured an Mg^{2+}-related speeding of Ca^{2+} release during photolysis of NP. We have used these data, plus data related to the relaxation of [Ca^{2+}] levels after photolysis, to constrain models of NP photolysis that include the kinetics of Mg^{2+} binding to both the unphotolyzed and photolyzed forms of the compound. This modeling then

TABLE 2 Rates for scheme 2

Ca-NP		Mg-NP		Ca-PP1		Mg-PP1 and PP2		Ca-PP2		Ca-F	
α_1	3.00×10^7	α_2	6.00×10^4	α_3	3.00×10^7	α_4	6.00×10^4	α_5	3.00×10^7	α_6	1.22×10^8
β_1	1.50×10^{-1}	β_2	1.50×10^{-1}	β_3	9.00×10^4	β_4	1.80×10^1	β_5	4.00×10^2	β_6	9.00×10^1
K_{d1}	5.00×10^{-9}	K_{d2}	2.50×10^{-6}	K_{d3}	3.00×10^{-3}	K_{d4}	3.00×10^{-3}	K_{d5}	1.33×10^{-5}	K_{d6}	7.30×10^{-7}

Values are given in the following units: α ($M^{-1}\ s^{-1}$); β (s^{-1}); K_d (M). The total concentrations used in the model were as follows (in mM): NP, 5.0; Ca^{2+}, 2.0; Mg^{2+}, 2.0; fura-2, 0.05. The photolysis rate, R, used to fit the data in the presence of Mg^{2+} was allowed to vary a small amount (0.245–0.2775) to account for exposure to exposure variability due to differences in defocusing.

provides a basis for directly predicting the kinetics and levels of Ca^{2+} produced by NP photolysis in the presence of physiological concentrations of Mg^{2+}. Such predicative power is important if one desires to use NP to manipulate Ca^{2+} for experiments where Mg^{2+} is either known, or expected to be, crucial for the process under study. Such experiments include studies of exocytosis (Gillis et al., 1996) and muscle contraction (Patel et al., 1996). An understanding of Mg^{2+} binding to NP is also important for predicting the Ca^{2+} levels produced by NP photolysis in systems where Mg^{2+} levels cannot be arbitrarily set to zero. This is true for experiments in microinjected cells (Delaney and Zucker, 1991; Mulkey and Zucker, 1993; Kamiya and Zucker, 1994; Landò and Zucker, 1994).

Choice of kinetic model

We initially tried to constrain Mg^{2+} binding within the context of a conventional model of NP photolysis (Scheme 1), but this model failed to describe our results. The expectation was that one could alter the Mg-NP binding rates such that Scheme 1 mimicked the slow recovery of Ca^{2+} levels after photolysis in the presence of Mg^{2+}. In fact, no amount of manipulation of the conventional model (Scheme 1) allowed it to follow the very slow recovery seen after longer photolysis episodes (Fig. 3, *B* and *C*).

This finding forced the development of a new model (Scheme 2) which produced different photoproducts dependent on whether the NP was originally complexed to Ca^{2+} or not. Although the data presented in the Modeling section suggest that the model alteration was made to satisfy the constraint of recovery in the presence of Mg^{2+}, there are additional reasons to expect such a mechanism for NP photolysis might be correct.

First, in the original description of NP, Kaplan and Ellis-Davies (1988) described the production of differentially absorbing species after photolysis. As in Scheme 2, the species produced was a function of whether the NP was photolyzed in the absence or presence of Ca^{2+}. Kaplan and Ellis-Davies (1988) only characterized the Ca^{2+} binding affinity of the photoproduct produced by photolysis in the presence of excess Ca^{2+}. The published affinity was 3 mM. The affinity of the species produced by photolysis in the absence of Ca^{2+} was not established.

Neher and Zucker (1993) reported a different value (250 μM) for the Ca^{2+} affinity of the NP photoproduct, assuming the production of a single photoproduct. We concur with this value; when using Scheme 1, which produces only a single photoproduct, this higher affinity is required to account for our data. The 3 mM photoproduct produces too high Ca^{2+} levels after photolysis and too fast changes in Ca^{2+} during long photolysis episodes.

This quandary thus leads to a second rationale for developing Scheme 2. The scheme reconciles the two different K_d values for the NP photoproduct. We propose that the 250 μM photoproduct is not "real." It is rather the apparent affinity of a mixture of the two photoproducts of Scheme 2, one with an affinity of 3 mM and the other with a much higher affinity (13.3 μM based on our modeling). The actual composition of the mixture is a function of the amount of NP bound to Ca^{2+} before photolysis. It is important to note that neither Kaplan and Ellis-Davies (1988) nor Neher and Zucker (1993) performed a Scatchard analysis, which might have detected multiple affinities. Rather, they measured the free Ca^{2+} after photolysis and used this value to predict the affinity of a single buffer species that would produce the measured Ca^{2+} level.

Adjusting the affinity of PP2 in Scheme 2 to fit the different steady Ca^{2+} levels after increasing length of photolysis episodes (Fig. 3) is in effect a method of titrating PP2. This was done within the context of a system of three other Ca^{2+} buffers (NP, PP1, and fura-2). Of these, only the K_d of NP has been relatively rigorously determined, so the value for the K_d of PP2 we have calculated, 13.3 μM, is only an approximation. Nevertheless, using fixed values for the K_d values of the other three buffers, it was not possible to vary the value of the K_d for PP2 by a factor of three and still fit all the data described in the present study.

By using Scheme 2 we were able to reach a single set of Mg-NP binding rates that produced reasonably good fits to the data presented in Fig. 3*, A–C*. As indicated above, the rates for the Mg-NP were highly constrained in this scheme, which allowed us to closely estimate values that fit our data.

As mentioned above, we also varied two other parameters in a minimal fashion to allow both Scheme 1 and Scheme 2 to more closely fit the data presented in Fig. 3. These two parameters were the value of R_{min} used in fura-2 calibration and the photolysis rate R used in the modeling. R_{min} was varied so the initial data calcium levels, measured by fura-2, matched the initial calcium levels predicted by the two schemes. Photolysis rate, R, was varied to make the peak calcium levels at the end of each photolysis episode match more closely. This necessity for variation in rate (6.2%) is believed to be a function of the variability in light levels and cuvette thicknesses among the various exposures. While both these parameters were varied to maximize fitting, the necessity of using Scheme 2 rather than Scheme 1, and the Mg-NP binding rates chosen for the best fit using Scheme 2, would not be altered if these minor corrections were not made.

We considered a third model in which NP photolyzes to a high Ca^{2+}-affinity intermediate. The intermediate then spontaneously degrades to a final photoproduct. As indicated, this model was discarded, primarily because there was no known chemical evidence for a long-lasting intermediate. It is of some interest, however, that the best fits of this model to our complete data set occurred as the spontaneous breakdown rate was made increasingly small. In the limit, when spontaneous breakdown ceases, this type of model becomes very much like the most important aspect of Scheme 2, photolysis to a stable high-affinity intermediate. This finding is indirect support of Scheme 2.

Until now we have considered only schemes in which DM-nitrophen is photolyzed at rates independent of whether it is free or bound to Ca^{2+} or Mg^{2+}. Previous estimates of Ca-NP and NP photolysis rates indicated that Ca-NP is photolyzed 2.5 times faster that NP (Zucker, 1993). However, this conclusion was based on measurements of Ca-NP and NP absorbance changes during photolysis, and did not consider the production of different photoproducts included in our Scheme 2 and indicated by Kaplan and Ellis-Davies (1988), nor did it consider the possibility of the further photolysis of the initial photoproducts. These complications call into question the interpretation of the data used to conclude that there are different photolysis rates for NP and Ca-NP.

We have addressed the possibility that NP is photolyzed more slowly than Ca-NP (and Mg-NP) by running simulations of a variation of Scheme 2 with different photolysis rates. Assuming that Ca-NP (and Mg-NP) are photolyzed 2.5 times faster than NP gave a somewhat worse fit to the data of Fig. 3, and resulted in estimates of $\alpha_2 = \alpha_4 = 3 \times 10^4\ M^{-1}\ s^{-1}$, $\beta_2 = 0.075\ s^{-1}$, $\beta_4 = 9\ s^{-1}$, $K_{d5} = 20\ \mu M$, and $\beta_5 = 60\ s^{-1}$. This model thus has little effect on estimates of the Mg^{2+} binding rates of NP, and of the affinity of the photoproduct formed from free NP. Although we cannot exclude this model, in the absence of independent evidence for different photolysis rates for NP vs. Ca-NP and Mg-NP we prefer to use the parameters from the simpler and better-fitting version of Scheme 2 with a single photolysis rate.

Possible errors and limitations of the present study

As indicated above, the value for the Ca^{2+} affinity of PP2 in Scheme 2 ($K_{d5} = 13.3\ \mu M$) should be taken as preliminary. The K_{d5} providing the best fit of the data is a function of the relative Ca^{2+} affinities for the several other buffers present, including fura-2 and NP. Thus, a slightly different value for the fura-2 K_d, which is not unexpected given the inherent noise in fura-2 calibrations, would change the value for K_{d5}. The fura-2 calibration breaks down at the higher values of calcium reached in the long exposure of Fig. 4. Thus, these data were not used to constrain K_{d5} or the rest of the model, but rather as a test of the model as constrained by the data in Fig. 3.

There are two possible sources of error in the recovery time course data that deserve discussion. First, we must consider the possibility that diffusion related changes are still present in the recovery data. This seems unlikely for several reasons. We carefully determined a set of photolysis parameters that minimized, if not eliminated, diffusion-related artifacts. We are measuring recovery within a time window of 2–3 s after the termination of photolysis. Our measurements and calculations suggest that diffusion will not become a factor until time periods near 10 s. Other records, with longer photolysis and recovery times, were not used in the present study because they showed a slow recovery after photolysis that was consistent with a diffusional process. The extended photolysis data in Fig. 4 may show the effect of diffusion in the latter part of the record.

The second artifact that might affect recovery data is additional photolysis occurring during the recovery pulses. In the worst case, after the 1.0-s exposures, 10-ms monitoring pulses would photolyze $<1\%$ additional NP. The quantitative recovery experiments were done under conditions of reduced photolysis efficiency by using an iris diaphragm and by defocusing to cut back light levels.

Our results provide information needed in predicting the effects of NP photolysis in cells containing Mg^{2+}. Scheme 2 is a model that describes our full range of results in the presence of Mg^{2+}, and can be used to predict what will happen to $[Ca^{2+}]$ in cells in response to a light exposure (or flash) of known duration and intensity (or measured photolysis efficiency). This is important in designing experiments using NP to regulate $[Ca^{2+}]$. To accurately estimate the effects of photolysis in a living cell, it is necessary to know concentrations of total Ca^{2+}, NP, and Mg^{2+}, as well as amounts and binding kinetics and affinities of other Ca^{2+} and Mg^{2+} buffers (such as cytoplasmic proteins and ATP) and rate of Ca^{2+}-extrusion processes. There is often sufficient information to estimate all these processes (e.g., Xu et al., 1997), in which case fairly precise predictions of effects of photolysis can be made, and experimental protocols designed to achieve the desired effects. Our model scheme can then be a useful tool in the quantitative experimental manipulation of intracellular $[Ca^{2+}]$.

This research was supported by National Institutes of Health Research Grant NS 15114. R.S.Z. was supported by the Miller Institute for Basic Research in Science.

REFERENCES

Adams, S. R., J. P. Y. Kao, G. Grynkiewicz, A. Minta, and R. Y. Tsien. 1988. Biologically useful chelators that release Ca^{2+} upon illumination. *J. Am. Chem. Soc.* 110:3212–3220.

Bers, D. M. 1982. A simple method for the accurate determination of free [Ca] in Ca-EGTA solutions. *Am. J. Physiol.* 242:C404–C408.

Cash, S., Y. Dan, M.-M. Poo, and R. Zucker. 1996. Postsynaptic elevation of calcium induces persistent depression of developing neuromuscular synapses. *Neuron.* 16:745–754.

Delaney, K. R., and R. S. Zucker. 1990. Calcium released by photolysis of DM-nitrophen stimulates transmitter release at squid giant synapse. *J. Physiol.* 426:473–498.

Ellis-Davies, G. C., and J. H. Kaplan. 1994. Nitrophenyl-EGTA, a photolabile chelator that selectively binds Ca^{2+} with high affinity and releases it rapidly upon photolysis. *Proc. Natl. Acad. Sci. USA.* 91:187–191.

Ellis-Davies, G. C., J. H. Kaplan, and R. J. Barsotti. 1996. Laser photolysis of caged calcium: rates of calcium release by nitrophenyl-EGTA and DM-nitrophen. *Biophys. J.* 70:1006–1016.

Escobar, A. L., F. Cifuentes, and J. L. Vergara. 1995. Detection of Ca^{2+}-transients elicited by flash photolysis of DM-nitrophen with a fast calcium indicator. *FEBS Lett.* 364:335–338.

Escobar, A. L., P. Velez, A. M. Kim, F. Cifuentes, M. Fill, and J. L. Vergara. 1997. Kinetic properties of calcium indicators: rapid transient responses to flash photolysis of DM-nitrophen. *Pflügers Arch.* 434: 615–632.

Gillis, K. D., R. Mossner, and E. Neher. 1996. Protein kinase C enhances exocytosis from chromaffin cells by increasing the size of the readily releasable pool of secretory granules. *Neuron.* 16:1209–1220.

Grynkiewicz, G., M. Poenie, and R. Y. Tsien. 1985. A new generation of Ca^{2+} indicators with greatly improved fluorescence properties. *J. Biol. Chem.* 260:3440–3450.

Hague, D. N. 1977. Dynamics of substitution at metal ions. *Molec. Biol. Biochem. Biophys.* 24:84–106.

Heidelberger, R., C. Heinemann, E. Neher, and G. Matthews. 1994. Calcium dependence of the rate of exocytosis in a synaptic terminal. *Nature.* 371:513–515.

Henke, W., C. Cetinsoy, K. Jung, and S. Loening. 1996. Non-hyperbolic calcium calibration curve of Fura-2: implications for the reliability of quantitative Ca^{2+} measurements. *Cell Calcium.* 20:287–292.

Jackson, A. P., M. P. Timmerman, C. R. Bagshaw, and C. C. Ashley. 1987. The kinetics of calcium binding to fura-2 and indo-1. *FEBS Lett.* 215:35–39.

Kamiya, H., and R. S. Zucker. 1994. Residual Ca^{2+} and short-term synaptic plasticity. *Nature.* 371:603–606.

Kao, J. P. Y., and R. Y. Tsien. 1988. Ca^{2+} binding kinetics of fura-2 and azo-1 from temperature-jump relaxation measurements. *Biophys. J.* 53: 635–639.

Kaplan, J. H., and G. C. Ellis-Davies. 1988. Photolabile chelators for the rapid photorelease of divalent cations. *Proc. Natl. Acad. Sci. USA.* 85:6571–6575.

Landò, L., and R. S. Zucker. 1989. "Caged calcium" in *Aplysia* pacemaker neurons. Characterization of calcium-activated potassium and nonspecific cation currents. *J. Gen. Physiol.* 93:1017–1060.

Landò, L., and R. S. Zucker. 1994. Ca^{2+} cooperativity in neuroexcretion measured using photolabile Ca^{2+} chelators. *J. Neurophysiol.* 72:825–830.

Mulkey, R. M., and R. S. Zucker. 1993. Calcium released by photolysis of DM-nitrophen triggers transmitter release at the crayfish neuromuscular junction. *J. Physiol.* 462:243–260.

Neher, E., and R. S. Zucker. 1993. Multiple calcium-dependent processes related to secretion in bovine chromaffin cells. *Neuron.* 10:21–30.

Neveu, D., and R. S. Zucker. 1996. Postsynaptic levels of $[Ca^{2+}]_i$ needed to trigger LTD and LTP. *Neuron.* 16:619–29.

Parsons, T. D., J. R. Coorssen, H. Horstmann, and W. Almers. 1995. Docked granules, the exocytic burst, and the need for ATP hydrolysis in endocrine cells. *Neuron*. 15:1085–1096.

Parsons, T. D., G. C. Ellis-Davies, and W. Almers. 1996. Millisecond studies of calcium-dependent exocytosis in pituitary melanotrophs: comparison of the photolabile calcium chelators nitrophenyl-EGTA and DM-nitrophen. *Cell Calcium.* 19:185–192.

Patel, J. R., G. M. Diffee, and R. L. Moss. 1996. Myosin regulatory light chain modulates the Ca^{2+} dependence of the kinetics of tension development in skeletal muscle fibers. *Biophys. J.* 70:2333–2340.

Thomas, P., J. G. Wong, A. K. Lee, and W. Almers. 1993. A low affinity Ca^{2+} receptor controls the final steps in peptide secretion from pituitary melanotrophs. *Neuron.* 11:93–104.

Tsien, R. Y., and R. S. Zucker. 1986. Control of cytoplasmic calcium with photolabile tetracarboxylate 2-nitrobenzhydrol chelators. *Biophys. J.* 50:843–853.

Xu, T., M. Naraghi, H. Kang, and E. Neher. 1997. Kinetic studies of Ca^{2+} binding and Ca^{2+} clearance in the cytosol of adrenal chromaffin cells. *Biophys. J.* 73:532–545.

Zucker, R. S. 1992. Effects of photolabile calcium chelators on fluorescent calcium indicators. *Cell Calcium.* 13:29–40.

Zucker, R. S. 1993. The calcium concentration clamp: spikes and reversible pulses using the photolabile chelator DM-nitrophen. *Cell Calcium.* 14:87–100.

Zucker, R. S. 1994. Photorelease techniques for raising of lowering intracellular Ca^{2+}. *Methods Cell Biol.* 40:31–63.